ANALYSIS OF TURBULENCE AND NOISE EMISSION IN OPEN RECTANGULAR CAVITY AND SEPARATED FLOWS

T. Gandhi[a], C. Airiau[a], T. Poinsot[a], A. Kourta[b]

[a]Université de Toulouse, INPT, UPS, CNRS, IMFT,
Allée du Professeur Camille Soula, 31400, Toulouse, France
[b]ESA/Institut PRISME, Polytech'Orléans, 8 Rue Leonard de Vinci, 45072, Orléans, France

ABSTRACT

Large eddy simulation coupled with Curle's acoustic analogy was performed on the two dimensional shallow rectangular cavity with thick incoming turbulent boundary layer. The aim of the work is to resolve the acoustics generated from the cavities of the terrestrial and air borne civilian vehicles. Three test cases with low Mach number $0.017, 0.058, 0.117$ are performed on the cavity of aspect ratio $L/D = 4$ with power law or equilibrium turbulent boundary layer as inflow conditions. Turbulent fluctuations, energy spectra and noise emission are discussed.

1. INTRODUCTION

Open cavity flows can be found in many aerospace configurations, particularly on aircraft wings and landing systems. Self-sustained oscillations linked to a complex feedback mechanism of shear layer instability impinging on the downstream corner of the cavity generates unnecessary noise. The main frequency is given by the Rossiter's formula. Cavities are also responsible for the increase of drag. They are therefore of interest for turbulence, flow separation and aeroacoustic analysis. The complexity of the phenomenon occurring in such a flow depends on the geometry characteristics (ratio length L/depth D) and on the characteristics of the incoming boundary layer. A large literature exists on this subject.

Here the flow on the 2D rectangular cavity with $L/D = 4$ with an incoming turbulent boundary layer is investigated. One interesting aspect of the study is the large momentum thickness θ of the incoming boundary layer. In this case where the Mach number ($M_\infty < 0.3$) is low, strong shear stresses are present in the cavity and the impingings of the eddies on the downstream edge and corner of the cavity generate large turbulent structures which interact with the downstream boundary layer, inducing large unsteady separations. Initially, the flow is solved using Large Eddy Simulation and then noise emission is given by Curle acoustic analogy [1]. This work is the initial step to analyse more complex three dimensional rectangular and cylindrical cavity flows. The LES model is presented in section 2. The equilibrium boundary profile obtained from asymptotic analysis is explained in section 3. Section 4 discusses the aeroacoustic analogy model. The last section is devoted to the results of different configurations.

2. GOVERNING EQUATIONS AND NUMERICAL METHOD

2.1 Governing equations

The compressible Navier-Stokes equations in Cartesian coordinates without body forces or external heat addition can be written as

$$\frac{\partial U}{\partial t} + \frac{\partial E_j}{\partial x_j} = \frac{\partial F_{ij}}{\partial x_j}$$

where $U = [\rho, \rho u_i, \rho E_t]^T$ is the state vector, $E_j = [\rho u_j, \rho u_i u_j + p\delta_{ij}, \rho E_t u_j + p u_j]^T$ are the inviscid fluxes, $F_{ij} = [0, \tau_{ij}, \tau_{ij} u_i - q_j]^T$ are the diffusive fluxes and the viscous stress tensor is $\tau_{ij} = \mu \left(\frac{\partial u_i}{\partial x_j} + \frac{\partial u_j}{\partial x_i} - \frac{2}{3}\frac{\partial u_k}{\partial x_k}\delta_{ij} \right)$, where δ_{ij} is the Kronecker symbol. The heat flux from Fourier's heat law is given by $q_i = -\frac{c_p \mu}{Pr}\frac{\partial T}{\partial x_i}$ where c_p is the specific heat capacity at constant pressure, Pr is Prandtl number, $E_t = E + u_i u_i/2$ is the total energy, E is the internal energy

2.2 Numerical method – LES model

The parallel code AVBP from CERFACS, Toulouse, solves the laminar and turbulent compressible Navier-Stokes equations in two and three space dimensions. For prediction of unsteady turbulent flows, Direct Numerical Simulation (DNS) or Large Eddy Simulation (LES) can be employed. The numerical schemes in AVBP are based on the cell-vertex method which naturally ensures high compactness. The main convective schemes are a finite volume Lax–Wendroff type scheme (LW) and a finite element two-step Taylor-Galerkin scheme (TTGC) [2]. These two schemes are respectively 2^{nd} and 3^{rd} order in time and space. The diffusive scheme is a typical 2^{nd} order compact scheme. In this work we typically use quadrangle elements for space discretization. Time integration is fully explicit to maximize accuracy. The derivation of the new governing equations is obtained by introducing operators to the compressible Navier-Stokes equations. Unclosed terms arise during the derivation and need to be modeled for the problem to be solved. The operator in LES is a spatially localized time independent filter of given size, $\triangle$, to be applied to a single realization of the studied flow. At the same time, the unclosed terms in LES represents the physics associated with the small structures present in the flow. The LES predictions of complex turbulent flows are closer to the physics since large scale phenomena such as large vortex shedding and acoustic waves are embedded in the set of governing equations [3]. The filtered compressible Navier-Stokes equations exhibit sub-grid scale (SGS) tensors and vectors describing the interaction between the non-resolved and resolved motions. The influence of the SGS on the resolved motion is taken into account by a SGS model based on the introduction of a turbulent viscosity ν_t. Two LES models are used here. The first one is LES–Smagorinsky model $\nu_t = (C_S\triangle)^2\sqrt{2\,\widetilde{S_{ij}}\widetilde{S_{ij}}}$, where $C_S = 0.18$ is the model constant and $\widetilde{S_{ij}}$ is the resolved strain rate tensor. The second one is the filtered Smagorinsky model $\nu_t = (C_{SF})^2\sqrt{2\,HP(\widetilde{S_{ij}})HP(\widetilde{S_{ij}})}$, where $C_{SF} = 0.37$ is the model constant and $HP(\widetilde{S_{ij}})$ denotes the resolved strain rate tensor obtained from a high-pass filtered velocity field.

Compressible flows are characterized by waves whose physics is to be respected in numerical simulations. Characteristic boundary conditions allow for the correct treatment of waves impinging on the boundary of the computational domain. Poinsot and Lele [4] characteristic boundary conditions are applied on all configurations . To prevent the numerical oscillations in the region of high gradients, artificial viscosity is added. Schönfeld Lartigue Kaufmann sensor (SLK) [5] is used with values of 0.2 and 0.05 for the 2^{nd} and 4^{th} order respectively.

3. INFLOW EQUILIBRIUM TURBULENT BOUNDARY LAYER

The equilibrium turbulent boundary layer is determined by the successive complemetary expansion method [6] which consists in seeking contiguous asymptotic matches between the inner and the outer regions of an incompressible turbulent boundary layer. Just the key steps are reproduced in this paper.

3.1 Mixing length model

Across the boundary layer, the local shear stress is given by $\tau = \mu \dfrac{\partial u}{\partial y} - \rho \overline{u'v'} = \tau_l + \tau_t$,where u' and v' are the time-dependent fluctuations of the streamwise and flow-normal velocity components. The Reynolds shear stress τ_t is evaluated using Prandtl's mixing length model [7], with the Van Driest [8] near-wall damping correction $\tilde{\mathrm{F}}$:

$$\tau_t = \rho \tilde{\mathrm{F}}^2 \ell^2 \left| \frac{\partial u}{\partial y} \right| \left(\frac{\partial u}{\partial y} \right), \qquad \tilde{\mathrm{F}} = 1 - \exp\left(-y^+/26\right) \tag{1}$$

In the inner region, $\ell = \kappa y$, while in the outer region, $\ell/\delta \to 0.085$ as $y \to \delta$. These two trends can be merged analytically into a single distribution for the mixing length ℓ across the full boundary layer by the using a blending function. Michel et al. [9] proposed

$$\ell(\eta)/\delta = c_\ell \tanh(\kappa\eta/c_\ell), \qquad c_\ell = 0.085, \quad \kappa = 0.41 \tag{2}$$

To deliver an improved prediction of the turbulent shear stress profile at the interface between the inner and the outer layer, at low Reynolds numbers Re_τ, a new alternative function have been implemented

$$\ell(\eta)/\delta = \kappa\eta \left[1 + (\kappa\eta/c_\ell)^n\right]^{-1/n} \tag{3}$$

For $2.6 < n < 2.7$, the $\ell(\eta)$ profile from equation 3 almost matches that from equation 2.

3.2 Stress and velocity profiles

Normalising the local shear stress τ in eq. 1 by ρu_τ^2 and assuming a monotonic velocity profile gives

$$\frac{\tau}{\tau_w} = \frac{\partial u^+}{\partial y^+} + \ell^{+2}\tilde{\mathrm{F}}^2 \left(\frac{\partial u^+}{\partial y^+}\right)^2, \qquad \ell^+ = \ell u_\tau/\nu, \quad u^+ = u/u_e \tag{4}$$

In the inner region and in the limit $y^+ \to 0$, $\tau \to \tau_w$ the root [6] of eq. 4 is

$$\frac{\partial u^+}{\partial y^+} = \frac{2}{1 + \sqrt{1 + 4\left[\ell^+\left(y^+\right)\tilde{\mathrm{F}}\left(y^+\right)\right]^2}} \tag{5}$$

Integrating equation 5 with respect to y^+ with the boundary condition $u^+(x, 0) = 0$ gives the inner layer tangential velocity profile that asymptotes to the log-law. In the outer region, a similarity solution is sought in terms of the velocity defect $F'(\eta) = (u_e - u)/u_\tau$. Expressing τ/τ_w as a function of F and η gives [6]

$$\frac{\tau}{\tau_w} = \left(\frac{\ell}{\delta}\right)^2 F''^2 = 1 - \frac{F}{F_1} + \left(\frac{1}{F_1} + 2\beta\right)\eta F' \tag{6}$$

where

$$F = \int_0^\eta F'(\xi)\, d\xi; \quad F_1 = F(1); \quad \beta = -\frac{\delta}{u_\tau}\frac{du_e}{dx} \tag{7}$$

In the outer region, the Reynolds stress component is dominant over the laminar shear stress, so $\tau \simeq \tau_t$. From eq. 1, noting that the van Driest damping constant $\tilde{\mathrm{F}} \to 1$ at $y^+ \geq 100$, $\tau/\tau_w = (\ell/\delta)^2 F''^2$, where $F'' = dF'/d\eta$.

3.3 *Asymptotic matching of the inner and outer profiles*

A matching condition is sought for the velocity profiles of the inner and outer regions. Considering eq. 5 in the limit $y^+ \to \infty$ and eq. 6 in the limit $\eta \to 0$ give respectively [6]

$$
\begin{aligned}
u^+ &= \kappa^{-1} \ln y^+ + C && (8)\\
u_e^+ - u^+ &= -\kappa^{-1} \ln \eta + D_v && (9)
\end{aligned}
$$

The addition of the both equations gives the ratio u_e/u_τ [6] :

$$
u_e^+ = \kappa^{-1} \ln \frac{u_\tau \delta}{\nu} + C + D_v \qquad (10)
$$

Equation 10 provides the wall skin friction coefficient $C_f = \tau_w / \left(0.5 \rho u_e^2\right)$:

$$
(C_f/2)^{-1/2} = \kappa^{-1} \ln \frac{u_\tau \delta}{\nu} + C + D_v \qquad (11)
$$

The numerical implementation of the full problem resolution is detailed in [10]. The shape factor and the boundary layers thicknesses and the ratio R_θ/R_τ are then determined. The new mixing length model (eq. 3) has been validated with some experimental data, for a value $n = 4$, on zero pressure gradient turbulent boundary layer (fig. 1).

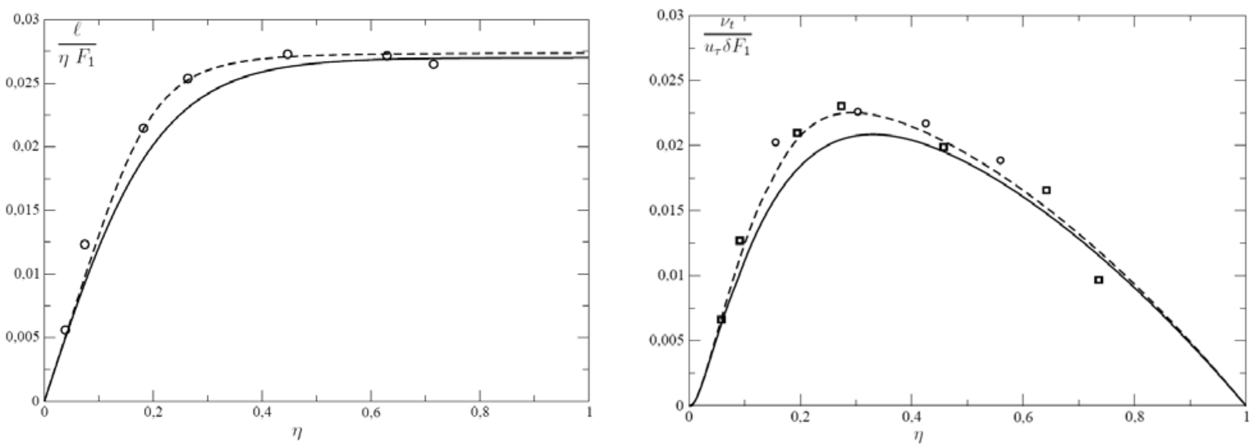

(a) Mixing length versus normalized η.

(b) Normalized eddy viscosity versus normalized distance η

Figure 1: reference data ○: $R_\tau = 1540$ [11], □ : $R_\tau = 2775$ [12], continuous line : results with Michel's model, dashed line : results with the model eq. 3, $n = 4$.

4. AEROACOUSTICS

Computational Aeroacoustics (CAA) aims to predict the sound radiated by turbulent flows, to identify the source of sound and to investigate strategies by which noise could be reduced. CAA combines the classical approaches of flow field computation with acoustics. The direct computation of sound using DNS is restricted to low Reynolds numbers and very simple geometries. Hybrid method where the sound is obtained in a successive step, after having calculated the flow field is employed as found in Lighthill [13] where an analogy between the propagation of sound in an unsteady unbounded flow to that in an uniform medium at rest, generated by a distribution of quadrapole acoustic sources. In this analogy, Navier-Stokes equations are replaced by an inhomogeneous wave equation namely the Lighthill equation. The Lighthill analogy does not include the effect of solid boundaries in the flow, thus it considers only aerodynamically generated sound without solid body interaction. The formulation was extended by Curle [1] and Ffows Williams and Hawkins [14] to take into account the generation and the scattering mechanisms when solid bodies are present:

$$\frac{\partial^2 \rho}{\partial t^2} - a_\infty^2 \frac{\partial^2 \rho}{\partial x_i^2} = \frac{\partial^2 T_{ij}}{\partial x_i \partial x_j} \tag{12}$$

where $T_{ij} = \rho u_i u_j - \tau_{ij} + (p - a_\infty^2 \rho)\delta_{ij}$ is the Lighthill stress tensor and a_∞ is the speed of sound in air. The equation (12) includes all physics as no assumption is made in deriving it from the governing equations. When an assumption of an inhomogeneous wave equation in an isotropic medium at rest is made and while assuming $\rho \sim \rho_\infty$ in T_{ij}, the equation (12) can be solved analytically. Curle [1] formulated an analogy for non-moving solid bodies using a general solution of equation (12)

$$\rho(\mathbf{x}, t) - \rho_\infty = \frac{1}{4\pi a_\infty^2} \int_V \frac{1}{r} \frac{\partial^2 T_{ij}}{\partial x_i \partial x_j} dV(\mathbf{y}) - \frac{1}{4\pi} \int_S \left(\frac{1}{r} \frac{\partial \rho}{\partial n} + \frac{1}{r^2} \frac{\partial r}{\partial n} \rho + \frac{1}{a_\infty r} \frac{\partial r}{\partial n} \frac{\partial \rho}{\partial \tau} \right) dS(\mathbf{y}) \tag{13}$$

where $\mathbf{x}$ is the observer position, $\mathbf{y}$ is the source position and $r = \mid \mathbf{x} - \mathbf{y} \mid$ is the distance between them. The vector n is the surface normal pointing towards to fluid and $\tau = t - r/a_\infty$ is the retarded time, which is the time of the emission of a signal that reaches the observer location at time t. After handling the equation (13) with Green's function and considering the observer located in a region where the flow is isentropic, the final surface integral is a line integral along the cavity walls yielding

$$p(\mathbf{x}, t) - p_0 = \frac{1}{4\pi} \int_L l_i n_j \left[2 \arctan(b/r) \frac{\dot{p}\delta_{ij}}{a_\infty} + 2b \frac{p\delta_{ij}}{r^2} \right] dL(\mathbf{y}) \tag{14}$$

where l_i is an unit vector pointing from the source to the observer, $\dot{p}$ is temporal derivative of pressure. At low Mach numbers [15] and [16] the surface integral term in the equation (13) is larger than the volume integral part, therefore the volume integral can be neglected. The results presented in this work use equation (14), which takes into account the real half width (b) of the cavity.

5. SIMULATION CHARACTERISTICS

testcase	U_∞	M_∞	Re_D	δ[mm]	θ[mm]	Re_θ	L/θ	at inlet
$U20$	$20\ m/s$	0.058	13.68×10^3	21.92	2.133	2920	18.75	MTBL
$U40$	$40\ m/s$	0.117	27.37×10^3	19.08	1.857	5100	21.54	MTBL
$U5.8$	$5.84\ m/s$	0.017	3.96×10^3	21.00	2.24	900	17.85	ETBL

Table 1: Flow parameters.

The computational domain extends between $0 \leq x/D \leq 25$ and $-1 \leq y/D \leq 20$. The cavity is between $5 \leq x/D \leq 9$ and $-1 \leq y/D \leq 0$. The dimensional variables which characterize the cavity flow [17] are L, D, free stream velocity U_∞, θ, a_∞, and kinematic viscosity ν_∞. The role played by the θ at the leading edge of the cavity in the selection of modes is observed by Colonius et al [18]. The flow parameters relevant to the cases in this work are given in the table 1. For test cases $U20$ and $U40$, a mean turbulent boundary layer (MTBL) is imposed at the intlet and a power law boundary layer profile is imposed on the whole computational domain as an initial condition. For the other test case $U5.8$, an equilibrium turbulent boundary layer (ETBL) was created by the method from the section 3. and imposed at the inlet and on the whole computational domain. All the three testcases were ran with the following flow state values : $P_0 = 101325\,Pa$, $T_0 = 288.15\,K$, $v_0 = 0\,m/s$. At the inflow, $\rho = \rho_\infty = 1.2kg/m^3$ and at the outflow, mean pressure $P = 101325\,Pa$ are imposed. The CFL value for these simulations is 0.7. The wall temperature is held constant and is equal to the free stream value $T_\infty = 288.15\,K$. For test cases $U20$ and $U40$ LES was performed with Smagorinsky model and for the test case $U5.8$, it was filtered Smagorinsky model. These computations are performed in parallel on 16 to 64 nodes of IBM-SP computers at IDRIS, Paris and on Altix 3700 computers at CALMIP, CICT, Toulouse.

6. RESULTS

6.1 Velocity profiles

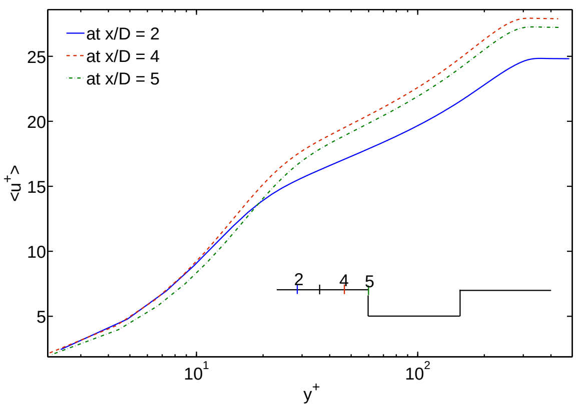

(a) $U_\infty = 5.8m/s$ at stations $x/D = 2, 4, 5$.

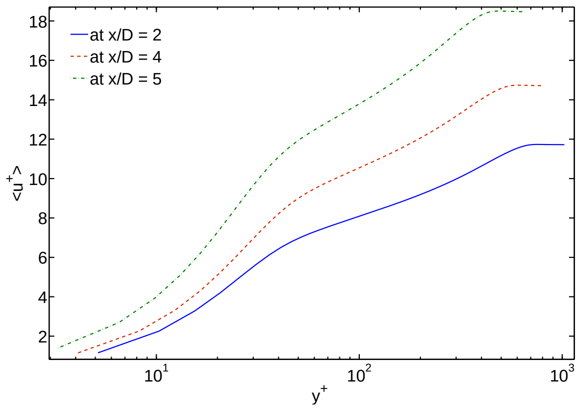

(b) $U_\infty = 20m/s$ at stations $x/D = 2, 4, 5$.

Figure 2: Boundary layer profiles for the test cases $U_\infty = 5.8m/s$ (a) and $U_\infty = 20m/s$ (b).

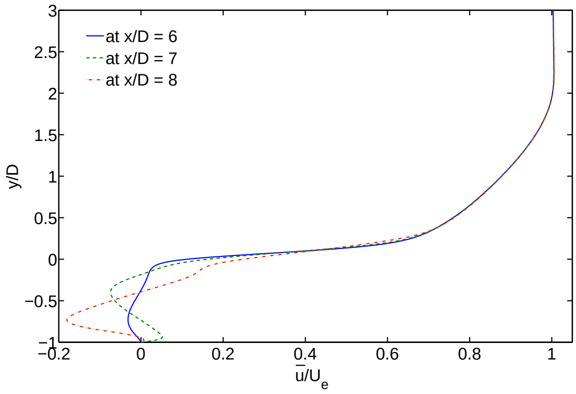

(a) $U5.8$ at stations $x/D = 6, 7, 8$.

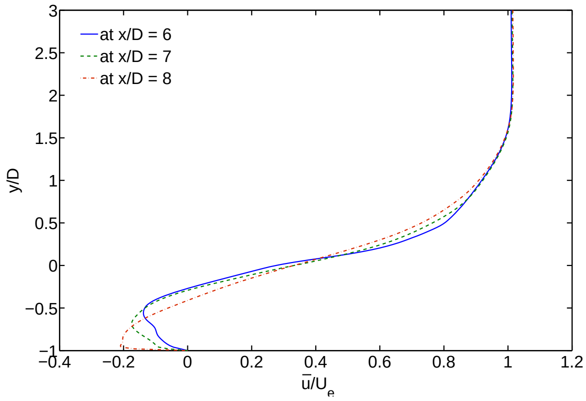

(b) $U20$ at stations $x/D = 6, 7, 8$.

Figure 3: Velocity profiles in the cavity of test cases $U5.8$ (a) and $U20$ (b).

The incoming boundary layer behaves like a flat plate boundary layer which can be observed in the figure 2. Time averaged velocity profiles in inner coordinates are plotted at stations

$x/D = 2, 4$, and 5. Comparison with asymptotic approach have demonstrated that in the section the boundary layer is no longer equilibrium. Typically the skin friction is lower than the theoretical value given by eq. 11. The discrepancy increases with the inlet mean velocity. For test cases $U20$ and $U40$, wake mode was observed. A vortex is formed from the leading edge of the cavity and fills the cavity region the vortex detaches and impinges on the downstream corner of the cavity. The flow above the cavity region is affected by the flow from the cavity. The free stream flow is periodically directed into the cavity. The flow was found to be highly unsteady and strongly influenced by the behaviour of the shear layer. Shear mode was observed for the test case $U5.8$.

The velocity profiles of x-component for the test cases $U5.8$ and $U20$ at stations $x/D = 6, 7, 8$ are shown in figures 3(a) and 3(b) respectively. The shear mode in the test case $U5.8$ is clearly evident from the figure 3(a) and the wake mode in the other testcase $U20$, figure 3(b).

6.2 Energy spectrum

The energy spectra of velocity component in x-direction versus the Strouhal number ($St_L = fL/U_\infty$,where f is frequency) for the test cases $U20$ and $U40$ are calculated at point $[x/D, y/D] = [8, 0]$ and are plotted in figures 4(a) and 4(b) respectively. The energy spectrum demonstrates the energy cascade where the peaks corresponding to the dominant oscillation frequency and its harmonics can be observed. The fundamental frequency for the test case $U40$ is $St_L = 0.205$, and all higher modes are harmonics of this fundamental frequency are observed in the figure 4(b). The fundamental frequency St_L reported by Larsson et al [15] is 0.245 which is worth mentioning here. Colonius et al [19] found a fundamental frequency of $St_L = 0.248$.

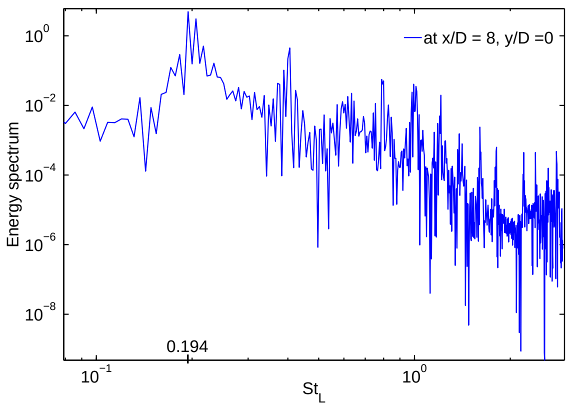

(a) $U_\infty = 20m/s$, at $x/D = 8, y/D = 0$.

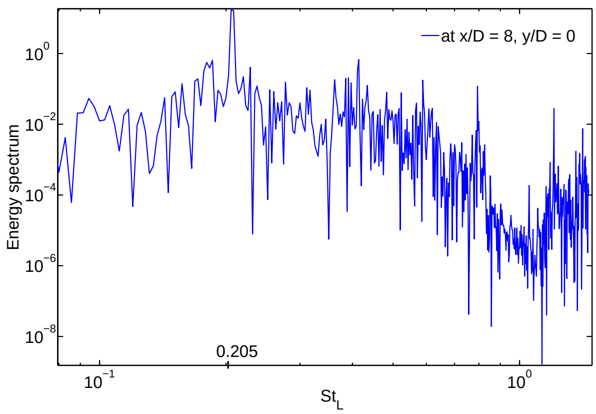

(b) $U_\infty = 40m/s$, at $x/D = 8, y/D = 0$.

Figure 4: Energy spectra of velocity component in x-direction of $U20$ (a) and $U40$ (b).

6.3 Reynolds stress profiles

In the figure 5, mean stresses $\overline{u'u'}$, $\overline{u'v'}$, $\overline{v'v'}$ profiles at $x/D = 2, 4$ and 5 resemble the usual turbulent boundary layer profiles. In the cavity at the locations $x/D = 6, 7$ and 8, mean stresses $\overline{u'u'}$, $\overline{u'v'}$, $\overline{v'v'}$ profiles are plotted and shown in the figure 6. The stress profiles of the test case $U5.8$ are qualitatively similar to profile from Bertier et al [20] and are typically from separated flows. The turbulent shear stress $\overline{u'v'}$ is directly linked with large eddies motion. So the anisotropic contribution to flow fluctuations is mostly distributed on the low frequency part of the spectrum. $\overline{u'u'}$ and $\overline{v'v'}$ may contribute more significantly to the high frequencies part.

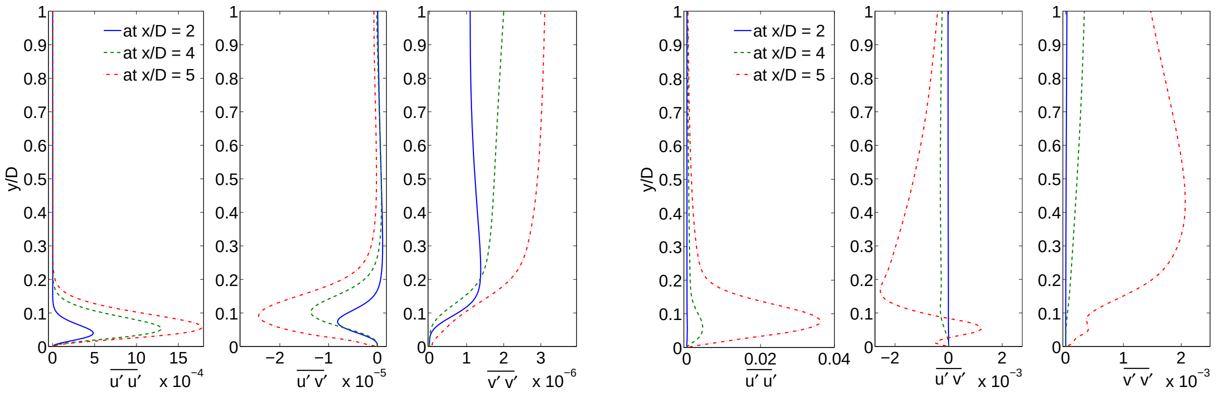

(a) $U_\infty = 5.8m/s$ (b) $U_\infty = 40m/s$

Figure 5: Mean stress profiles $\overline{u'u'}$, $\overline{u'v'}$ and $\overline{v'v'}$ at $x/D = 2, 4$ and 5.

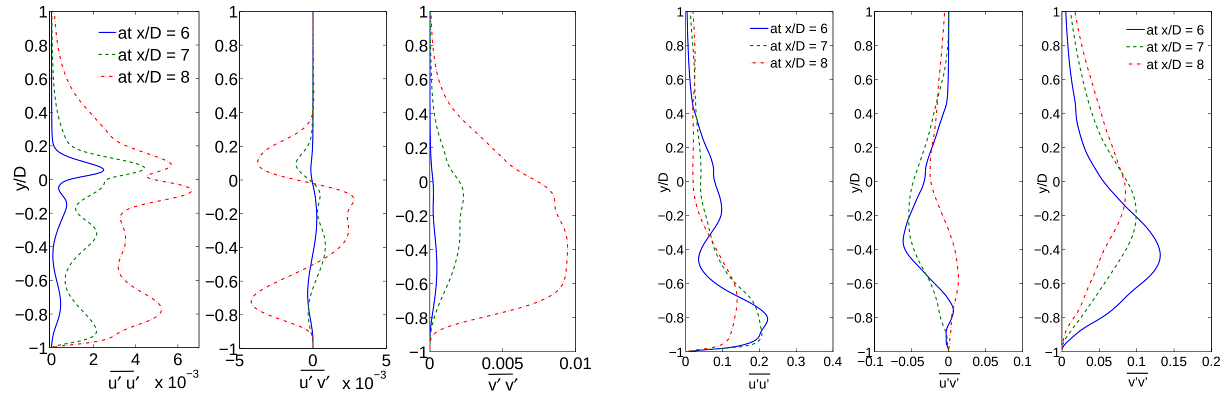

(a) $U_\infty = 5.8m/s$ (b) $U_\infty = 40m/s$

Figure 6: Mean stress profiles $\overline{u'u'}$, $\overline{u'v'}$ and $\overline{v'v'}$ at stations $x/D = 6, 7$ and 8 in the cavity.

6.4 Sound pressure level

As mentioned in the section 6.1, the interaction of the vortex with the trailing edge of the cavity generates pressure waves which are radiated into the far field. These pressure waves are identified as aerodynamic noise. To determine the SPL using the acoustic analogy, an acoustic domain of size $0 \leq x/D \leq 25$ and $-1 \leq y/D \leq 20$ with 50×50 grid points is generated. The intersection points of the grid represent the observers. The sound pressure level SPL values are calculated for both domains. The figure 7 shows SPL iso-contours, $SPL = 20\, log(p_{rms})/p_{ref}$ above the enclosure of the cavity, where $p_{ref} = 20\ \mu Pa$ and p_{rms} is the root mean square pressure fluctuation. The contour spacing is $\triangle SPL = 2\, dB$. SPL iso-contours appear to be concentric about the cavity, which confirms that the trailing edge is the main source of sound at the selected conditions. From the figure 7, at the trailing edge of the cavity, the maximum value of SPL is found to be $92dB$ for testcase $U5.8$ see figure 7(a) and $144dB$ for testcase $U40$ see figure 7(b) which confirms the louder flow. The direction of sound propagation appears uniform in the current cases of low Mach number shallow cavity flow with turbulent incoming boundary layer. But Rowley et al [21] show the peak radiation to the far field occurs at an angle of about 135° from the downstream axis for the cavity $L/D =$ and Mach number $M = 0.6$. But in the present case, the directivity angle is not prominent. The discrepancy may be due to

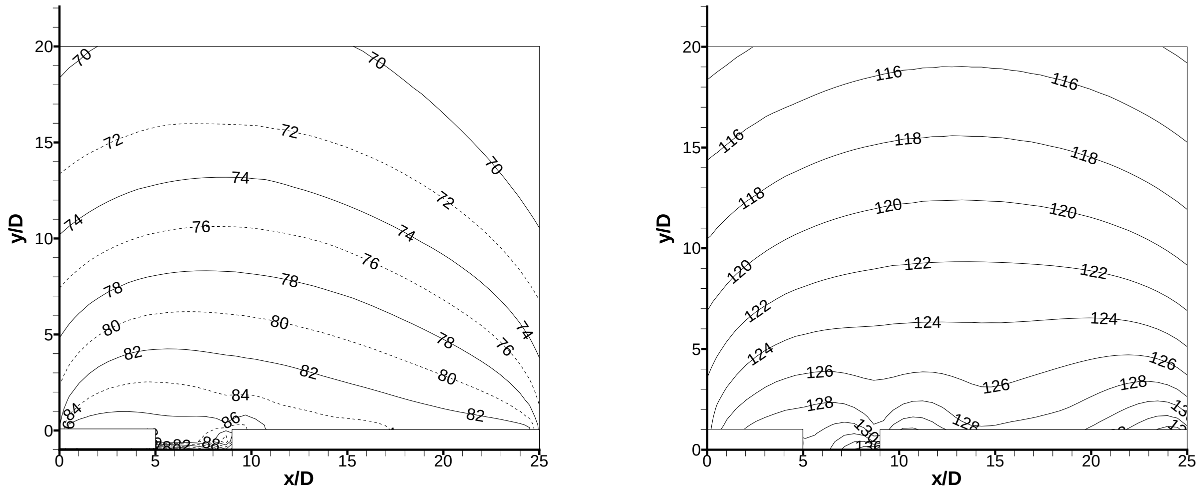

(a) SPL values in decibel for test case $U_\infty = 5.8m/s$ (b) SPL values in decibel for test case $U_\infty = 40m/s$

Figure 7: Sound Pressure Level

the low Mach number flow.

7. CONCLUSIONS

In this work, the LES has been used to investigate the nature of cavity mechanism and sound generation. The incoming flow with a mean turbulent boundary layer profile over a two dimensional cavities with $L/D = 4$ were simulated. The main sources of sound in this low Mach number flow are the pressure fluctuations on the walls. In addition, the sources of the sound are large on the downstream cavity wall. The differences in the directivity of the sound propagation is certainly an interesting part which should be studied in the future. The next step could be studying the turbulent $2D$ and $3D$ cavity flow with the unsteady inflow data imposed at the inlet.

ACKNOWLEDGEMENT

This research project AeroTraNet (www.imft.fr/aerotranet) has been supported by a Marie Curie Early Stage Research Training Fellowship of the European Community's Sixth Framework Programme under contract number MEST CT 2005 020301. We would like to thanks the IDRIS, Paris of the CNRS and CALMIP, CICT, Toulouse for providing the computing facilities for performing our calculations.

References

[1] N. Curle. The influence of solid boundaries upon aerodynamic sound. *Proc. Roy. Soc. Lond*, A23:505–514, 1955.

[2] Olivier Colin and Michael Rudgyard. Development of high-order Taylor-Galerkin schemes for LES. *Journal of Computational Physics*, 162, 2000.

[3] T. J. Poinsot and D. Veynante. *Theoretical & Numerical Combustion*. R T Edwards, 2001.

[4] T. J. Poinsot and S. K. Lele. Boundary conditions for direct simulations of compressible viscous flows. *Journal of Computational Physics*, 101:104–129, July 1992.

[5] O. Colin. *Simulation aux Grandes Echelles de la Combustion Turbulente Prémélangée dans les Statoréacteurs*. PhD thesis, Institut National Polytechnique de Toulouse, 2000.

[6] J. Cousteix and J. Mauss. *Asymptotic Analysis and Boundary Layers*. Springer-Verlag, Berlin Heidelberg, 2007.

[7] L. Prandtl. Bericht über untersuchungen zur ausgebildeten turbulenz. *Zeitschrift für angewandte Mathematik und Mechanik*, 5:136–139, 1925.

[8] E. R. Van Driest. On dimensional analysis and the presentation of data in fluid-flow problems. *ASME Journal of Applied Mathematics*, 13(1):34–40, Mar 1946.

[9] R. Michel, C. Quémard, and R Durant. Application d'un schéma de longueur de mélange à l'étude des couches limites turbulentes d'équilibre. Technical Note 154, ONERA, 1969.

[10] A. Rona, M. Grottadaurea, M. Monti, C. Airiau, and T. Gandhi. Generation of a turbulent boundary layer inflow for RANS simulations. In *15th AIAA/CEAS Aeroacoustics Conference (30th AIAA Aeroacoustics Conference)*, May 2009. AIAA 09-3272.

[11] P. S. Klebanoff. Characteristics of turbulence in a boundary layer with zero pressure gradient. Technical report, National Advisory Committee for Aeronautics (NACA), 1954.

[12] A. A. Townsend. Equilibrium layers and wall turbulence. *Journal of Fluid Mechanics*, 11:97–120, Aug 1961.

[13] M. J. Lighthill. On sound generated aerodynamically: I. General Theory. *Proceedings of the Royal Society of London, Series A*, 211:564–587, 1952.

[14] J. E. Ffowcs Williams and D. L. Hawkings. Sound generation by turbulence and surfaces in arbitrary motion. *Phil. Trans. of the Royal Soc.*, A264(1151):321–342, 1969.

[15] Johan Larsson, Lars Davidson, Lars-Erik Eriksson, and Magnus Olsson. Aeroacoustic investigation of an open cavity at low Mach number. *AIAA*, 42(12):2462–2473, 2004.

[16] Christian Haigermoser. *Investigation of cavity flows using advanced optical methods*. PhD thesis, Politecnico di Torino, 2009.

[17] Tim Colonius. An overview of simulation, modeling and active control of flow/acoustic resonance in open cavities. *AIAA paper*, 2001. 2001–0076.

[18] T. Colonius and S. K. Lele. Computational aeroacoustics:Progress on nonlinear problems of sound generation. *Progress in Aerospace Sciences*, 40(6):345–416, August 2004.

[19] T. Colonius, A. J. Basu, and C. W. Rowley. Computation of sound generation and flow/acoustics instabilities in the flow past an open cavity. In *Third ASME/JSME Joint Fluids Engg Conference*, 1999.

[20] N. Bertier, B. Courbet, D. Dutoya, F. Vuillot, and P. Sagaut. Large eddy simulation of a subsonic flow over a cavity on general unstructured grids. *AIAA*, 679, 2004.

[21] C. Rowley, T. Colonius, and A. Basu. On self-sustained oscillations in two-dimensional compressible flow over rectangular cavities. *Journal Fluid Mechanics*, 455:315–346, 2002.